Regular Article

Lattice-strain and electron-density modulation of palladium nanocatalysts for highly efficient oxygen reduction

Guojie Chao [a,b], Longsheng Zhang [a,*], Tiantian Xue [b], Jing Tian [b], Wei Fan [b], Tianxi Liu [a,b,*]

[a] Key Laboratory of Synthetic and Biological Colloids, Ministry of Education, School of Chemical and Material Engineering, International Joint Research Laboratory for Nano Energy Composites, Jiangnan University, Wuxi 214122, PR China
[b] State Key Laboratory for Modification of Chemical Fibers and Polymer Materials College of Materials Science and Engineering, Innovation Center for Textile Science and Technology, Donghua University, Shanghai 201620, PR China

GRAPHICAL ABSTRACT
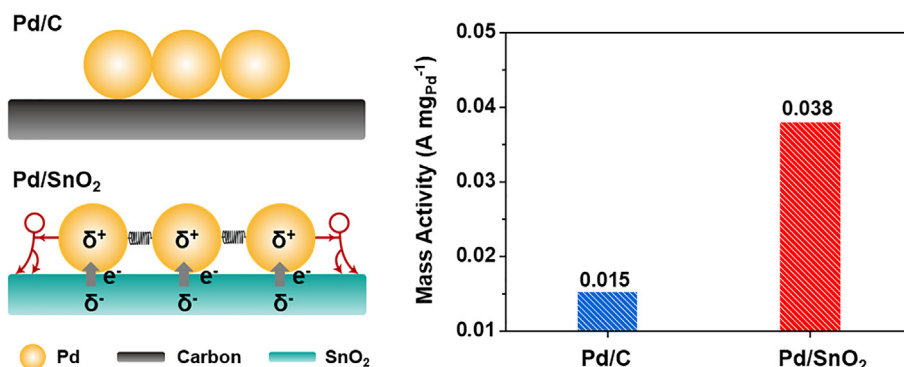
ARTICLE INFO

ABSTRACT

Designing efficient electrocatalysts for the oxygen reduction reaction (ORR) is crucial to enhance the energy efficiencies of metal-air batteries and fuel cells. Palladium (Pd) catalysts show great potential due to their high intrinsic activity towards ORR but suffer from inferior durability. Here, we aim to employ tin oxide (SnO_2) supports to tailor the lattice strain and electron density of Pd catalysts to enhance their ORR performance. By using electrospinning and solvothermal techniques, a hierarchical Pd/SnO_2 hybrid catalyst was facilely synthesized with Pd nanoparticles anchored onto both the inside and outside walls of nanotube-like SnO_2 supports. Owing to the SnO_2 supports and the endowing metal-support interactions, tensile-strain and electron-rich features were both verified for the Pd nanoparticles in the Pd/SnO_2 catalyst. In comparison, no such features were found for the Pd nanoparticles in the Pd/C catalyst. As a consequence, the Pd/SnO_2 hybrid catalyst exhibits 2.5-times higher mass activity than the Pd/C catalyst and greatly improved durability with a current decay of 4% loss over 50 h compared with that (18%) of the Pd/C catalyst.

---

* Corresponding authors at: Key Laboratory of Synthetic and Biological Colloids, Ministry of Education, School of Chemical and Material Engineering, International Joint Research Laboratory for Nano Energy Composites, Jiangnan University, Wuxi 214122, PR China.

E-mail addresses: zhangls@jiangnan.edu.cn (L. Zhang), txliu@jiangnan.edu.cn (T. Liu).

1. Introduction

Electrocatalytic oxygen reduction reaction (ORR) is widely used as the central cathodic reaction of metal-air batteries and fuel cells [1–5]. However, the sluggish kinetics of ORR remain a large obstacle to achieve high energy conversion efficiencies of metal-air batteries and fuel cells. Developing efficient ORR catalysts is crucial for promoting the development and application of these batteries and cells. Pt-based catalysts usually have the highest ORR activities, but their high cost and scarcity impede further advancement in practical applications [6–10]. Therefore, there is an urgent need to explore high-performance alternative ORR catalysts.

Recently, palladium (Pd) catalysts have attracted great attention as promising alternatives to platinum catalysts, owing to its similar electronic structure but lower cost [11–14]. Pd catalyst suffers from poor catalytic stability due to its high adsorption energies of oxygen-containing reaction intermediates [15–18]. Various strategies for constructing Pd-based alloys with additional transition metals have been adopted to improve the ORR performance. For instance, Guo et al. synthesized Pd-Mo alloys for ORR with high catalytic activity, where the alloying effects can tune the electronic structures of Pd active sites [19]. Feng et al. reported that Pd_6Ni alloys with core–shell structures exhibited improved ORR activity, where the surface Ni atoms can induce a downshift of the *d*-band center for weakening the oxygen absorption on the Pd (1 1 1) facet [20]. Indeed, higher ORR activities are achieved for the Pd-based alloys with optimized chemical compositions and electronic structures. Unfortunately, the catalytic durability improvements of these Pd-based alloys are limited owing to the unfavorable dealloying and dissolution of transition metal dopants during the ORR process [21–23].

Metal-support interactions in electrocatalysts are found to correlate with increased catalytic reaction kinetics, where the support can help to improve the supported metal electrocatalysts catalytic activities by modifying their electronic structures [24–28]. Notably, the semiconducting metal oxide supports can reduce the desorption energy of the O-containing intermediates at the active sites and facilitate their separation from the catalytic sites [29,30]. Tin oxide (SnO_2), a typical semiconductor metal oxide, has good electrochemical stability, nontoxicity and low cost and is considered as an ideal catalyst support [31–34]. We posit that constructing Pd/SnO_2 heterojunction catalysts may tailor the electronic structures and tune the adsorption energies of reaction intermediates on Pd metal sites, thereby enhancing the ORR activity and stability.

Herein, we report one facile approach to synthesize Pd/SnO_2 heterogeneous catalyst immobilizing Pd nanoparticles uniformly on the inner and outer walls of hollow SnO_2 nanotubes. Such hierarchical nanostructures can accelerate the reaction kinetics by increasing the electrolyte diffusion to access Pd active sites and induce strong metal-support interactions between Pd nanoparticles and SnO_2 supports. By combining transmission electron microscopy (TEM), X-ray diffraction (XRD) and X-ray photoelectron spectroscopy (XPS), we find that the Pd nanoparticles in an Pd/SnO_2 catalyst are subjected to tensile-strain and electron-rich features. However, these features cannot be found for Pd nanoparticles anchored onto a carbon support in a Pd/C catalyst. The electrochemical tests show that the Pd/SnO_2 catalyst exhibits 2.5-fold improvement in mass activity. Meanwhile, compared with the Pd/C catalyst, the electrochemical stability of the Pd/SnO_2 catalyst is improved. These results indicate that the SnO_2 supports and the endowing metal-support interactions play a significant role in boosting the ORR performance of the Pd/SnO_2 catalyst. This work provides a facile, scalable method to synthesize hierarchical Pd/SnO_2 catalysts, where strong metal-support interactions are induced to enhance the ORR activity and durability of the Pd/SnO_2 catalyst.

2. Materials and methods

2.1. Materials

Tin chloride dihydrate ($SnCl_2·2H_2O$, 98.0%), *N,N*-dimethylformamide (DMF, 99.0%) and ethanol (99.7%) were purchased from Shanghai Chemical Reagent Co., Ltd (China). Polyvinylpyrrolidone (PVP) (M.W. 1,300,000 and M.W. 10000), Nafion solution (5 wt%) and sodium tetrachloropalladate (Na_2PdCl_4, 98.0%) were purchased from Sigma-Aldrich (U.S.A). A commercial Pd/C (30 wt%) catalyst was obtained from Johnson-Matthey (China). Ethylene glycol (99.9%) was brought from Macklin (China).

2.2. Synthesis of the SnO_2 nanotubes

SnO_2 nanotubes were first prepared *via* an electrospinning technique [35]. Typically, $SnCl_2·2H_2O$ (1.2 g) was dissolved in a mixed solvent of DMF (5 mL) and ethanol (5 mL) under stirring for 4 h. Then, PVP (1.2 g, M.W. 1300000) was added to the above mixture and stirred for 12 h. The mixture was put in an injection syringe with a feeding rate of 0.25 mL min^{-1}. Electrospun $PVP/SnCl_2$ hybrid nanofibers were collected on a rotating aluminum collector at a voltage of 21 kV. The as-obtained electrospun membranes were placed in an oven at 80 ℃ for 5 h, and the resultant $PVP/SnCl_2$ hybrid membranes were annealed at 600 ℃ in air for 3 h to prepare the SnO_2 nanotubes.

2.3. Synthesis of the Pd/SnO_2 catalyst

The Pd/SnO_2 catalyst was prepared *via* a solvothermal method. First, the prepared SnO_2 nanotubes (40 mg) were dispersed in ethylene glycol (30 mL) in a vial through ultrasonication. The mixed solution was heated to 160 ℃ by using an oil bath. PVP (420 mg, M.W. 10000) and Na_2PdCl_4 (70 mg) were dissolved in ethylene glycol (3 mL) in two separate vials. Then, the PVP solution and the Na_2PdCl_4 solution were simultaneously added dropwise into the dispersion of SnO_2 nanotubes at 160 ℃. The mixture solution was maintained at 160 ℃ under stirring for another 1 h. The black precipitates were obtained through centrifugation and washing with ethyl alcohol 5 times. Finally, the black products were dried in a vacuum overnight.

3. Results and discussions

As shown in Fig. 1, we synthesized Pd/SnO_2 nanotubes *via* a facile approach by using electrospinning and solvothermal techniques. The phase structures of the obtained SnO_2 and Pd/SnO_2 samples were analyzed by XRD. In the XRD pattern of the obtained SnO_2 sample (Fig. S1), all characteristic peaks are found to be SnO_2 with a tetragonal phase. Meanwhile, the characteristic peaks of the obtained Pd/SnO_2 sample are mainly ascribed to metallic Pd in the face-centered cubic phase and SnO_2 in the tetragonal phase according to the XRD pattern. No diffraction peaks of impurities are found in their XRD patterns, indicating the successful preparation of the Pd/SnO_2 hybrid catalyst. Moreover, we further determined the Pd content in the Pd/SnO_2 samples by employing inductively coupled plasma-mass spectrometry measurements. The weight percentage of Pd was determined to be 10.4% in the Pd/SnO_2 catalyst.

The morphology of the SnO_2 and Pd/SnO_2 samples was further observed by scanning electron microscopy (SEM) and transmission electron microscopy (TEM). As shown in Fig. 2a and 2b, it is clearly revealed that the SnO_2 sample features a nanotube morphology according to the SEM and TEM observation results. Moreover, it
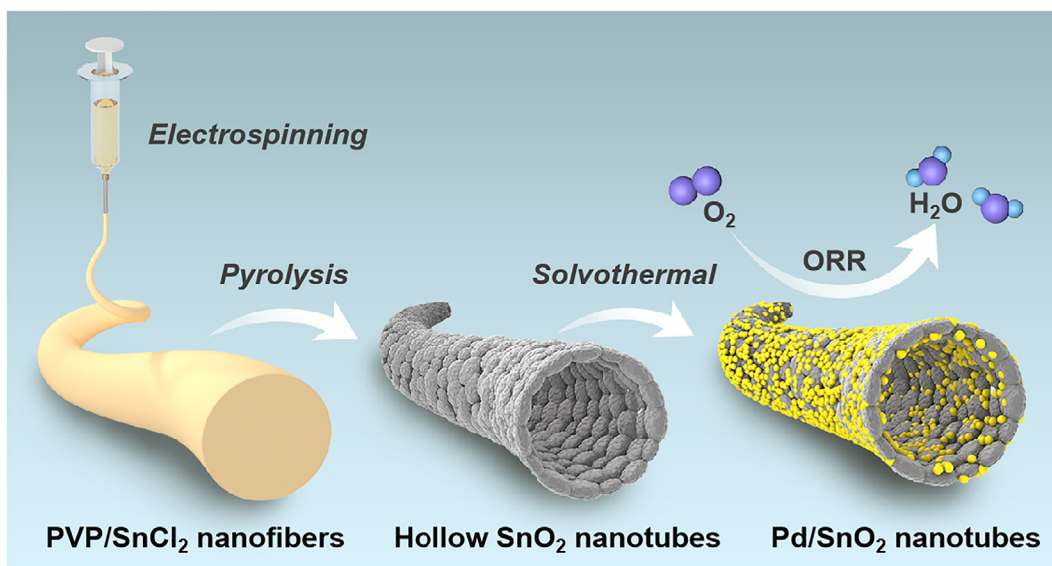
Fig. 1. Schematic of the synthesis of nanotube-like Pd/SnO₂ heterojunction catalysts for the electrocatalytic oxygen reduction reaction (ORR).
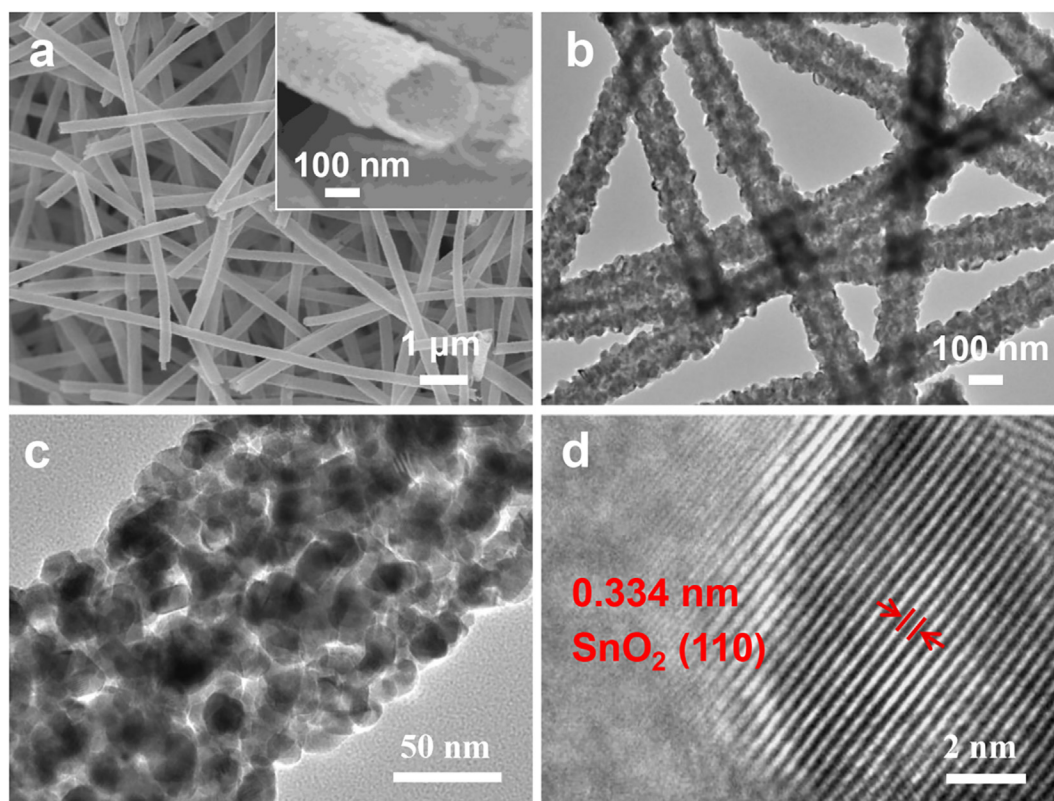

Fig. 2. (a) SEM and (b-d) TEM images of the obtained hollow SnO₂ nanotubes.

can be seen in the TEM image that one-dimensional SnO₂ nanotubes are formed with SnO₂ nanoparticles interconnected to each other (Fig. 2c). These hierarchical structures of the SnO₂ nanotubes show rough surfaces on both the inside and outside walls of the nanotubes to anchor the electroactive Pd nanoparticles, which effectively prevent agglomeration of Pd nanoparticles and enlarge the contact area to induce metal-support interactions between the SnO₂ support and Pd nanoparticles. The N₂ isothermal adsorption/desorption measurement (Fig. S2) shows that the SnO₂ sample

exhibits a typical-type IV isotherm with mesoporous characteristics, with a specific surface area of $8.4 \, m^3 \, g^{-1}$ and a pore size distribution of 11–25 nm. Furthermore, the (110) crystal plane of SnO₂ is clearly discovered in the TEM image of the SnO₂ nanotube (Fig. 2d), which is in agreement with the XRD results.

By using the SnO₂ nanotubes as supports, the Pd/SnO₂ sample was prepared by a one simple solvothermal method. The SEM images of the Pd/SnO₂ sample (Fig. 3a and 3b) show that its nanotube structure is well preserved after the solvothermal reaction.
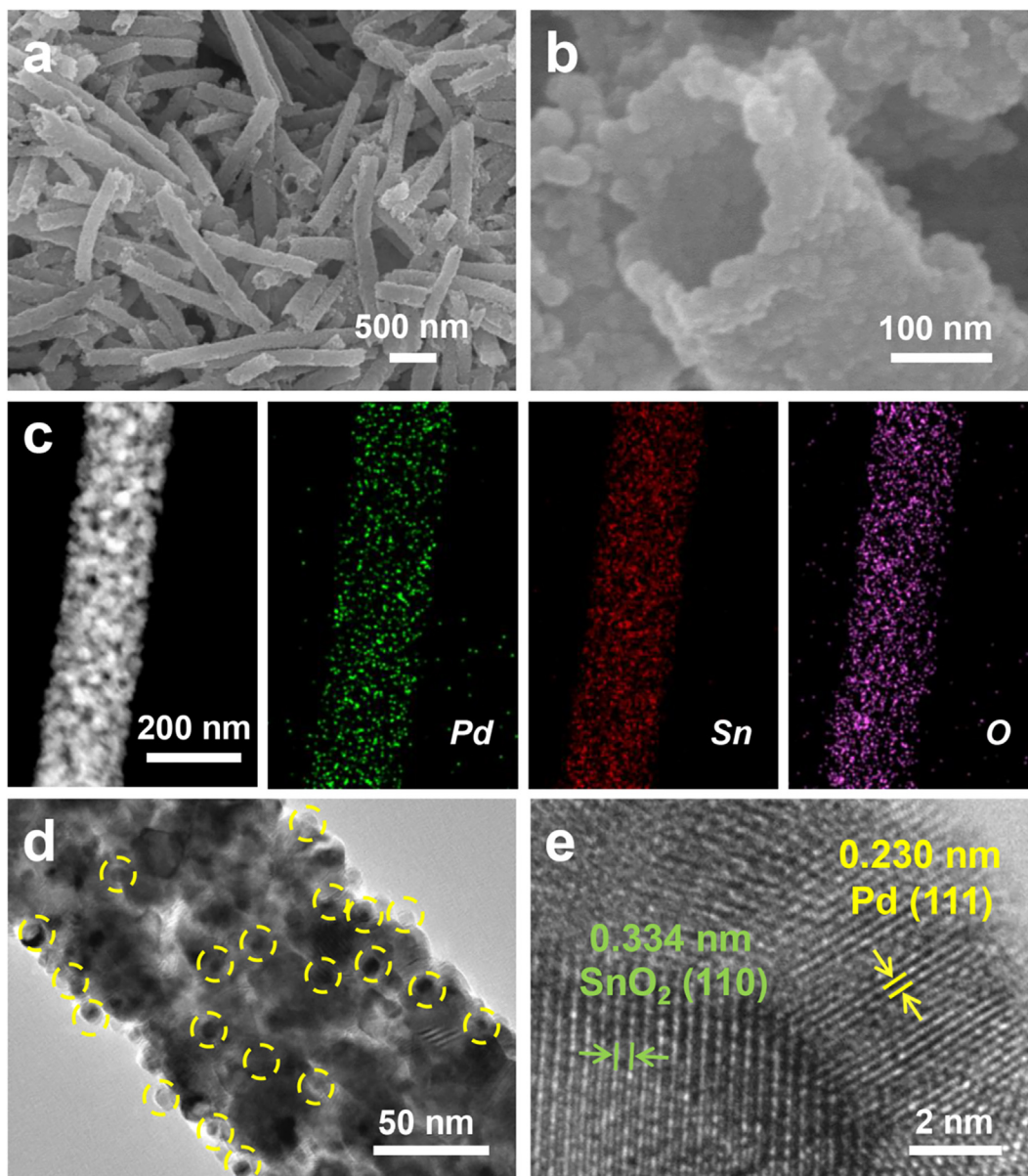
Fig. 3. (a, b) SEM images of the prepared Pd/SnO_2 sample. (c-e) TEM images and EDS mapping images of the Pd/SnO_2 sample.

As shown in Fig. 3c, the TEM and energy dispersive spectroscopy (EDS) images illustrate that the Pd, Sn and O elements are uniformly distributed in the Pd/SnO_2 nanotube. The TEM image of Pd/SnO_2 reveals that the Pd nanoparticles are uniformly anchored onto the SnO_2 nanotube with diameters of 6–10 nm (Fig. 3d). Especially, the (1 1 1) crystal plane of Pd and the (1 1 0) crystal plane of SnO_2 can be clearly observed in the TEM image (Fig. 3e). Notably, the lattice spacing (0.230 nm) of the Pd nanoparticles supported onto the SnO_2 nanotube is larger than that of metallic Pd (0.225 nm), indicating that the Pd nanoparticles in the Pd/SnO_2 sample are subjected to lattice tensile strain.

To investigate the influence of the lattice tensile strain of Pd nanoparticles on the catalyst support, the TEM comparison of the Pd/C and Pd/SnO_2 materials was carried out. Fig. S3 is the TEM images of the Pd/C sample, which demonstrate that Pd nanoparticles are anchored on the carbon support. Compared with the TEM images of the Pd/C (30%) and Pd/SnO_2 composites (Fig. 4a and 4b), the lattice spacing of the Pd nanoparticles in the Pd/C sample is similar to the theoretical lattice spacing of metallic Pd, but smaller

than that of the Pd nanoparticles in the Pd/SnO_2 sample. Moreover, we further integrated the pixel intensities of the Pd (1 1 1) facets selected from the TEM images of these two Pd-based samples. As shown in Fig. 4c and 4d, the Pd nanoparticles in the Pd/SnO_2 sample have a larger lattice distance than those in the Pd/C sample. The lattice spacing of the Pd nanoparticles anchored onto the SnO_2 supports is larger than that of the Pd nanoparticles anchored onto the carbon supports.

As shown in the XRD patterns of the above two Pd-based samples (Fig. 5a), the diffraction peak of Pd (1 1 1) of the Pd/SnO_2 sample is $\sim 39.9°$ while the diffraction peak of Pd (1 1 1) of the Pd/C sample is $\sim 40.1°$. Compared with the characteristic peak of standard Pd (1 1 1) ($2\theta = 40.1°$, PDF No. 46–1043), the diffraction peak of Pd (1 1 1) of the Pd/SnO_2 sample slightly shifts to a small diffraction angle. According to the Bragg equation ($d = n\lambda/2\sin\theta$, where d is the spacing of crystal faces; θ is the angle between the incident X-ray and the corresponding crystal plane; λ is the wavelength of the X-ray and n is the constant diffraction order), the smaller diffraction peak of Pd (1 1 1) verifies the existence of tensile strains
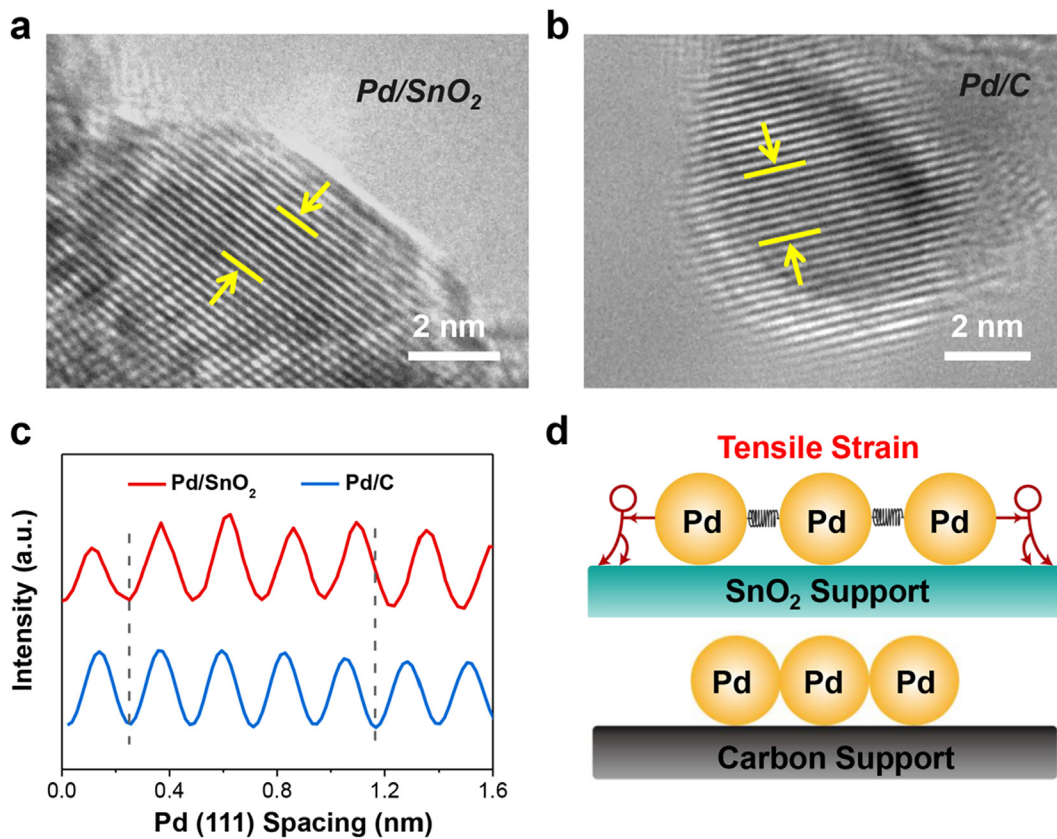
Fig. 4. (a–c) TEM images and corresponding integrated pixel intensities of Pd (1 1 1) lattices of Pd/SnO$_2$ and Pd/C, respectively. (d) Schematic of the generated tensile strains of the Pd (1 1 1) lattice on the SnO$_2$ support compared with the carbon support.
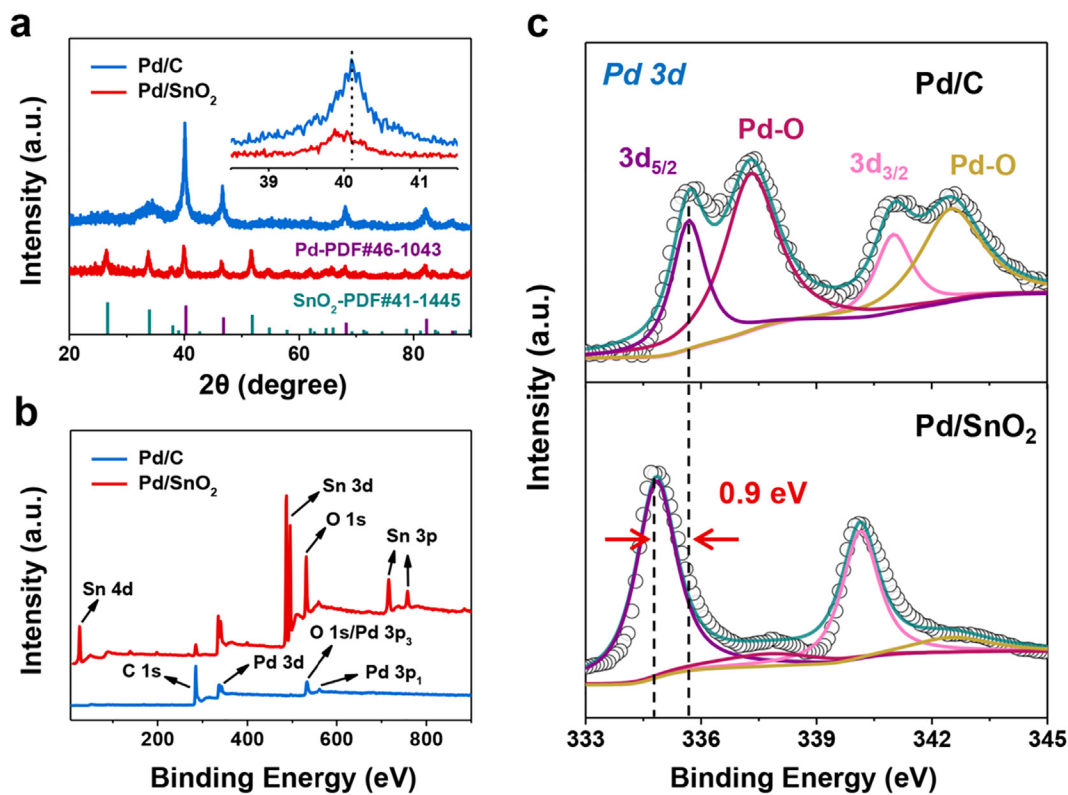

Fig. 5. (a–c) XRD patterns, XPS survey spectra and high-resolution Pd 3d spectra of Pd/C and Pd/SnO$_2$.

in the Pd nanoparticles for the Pd/SnO$_2$ sample, which is in agreement with the TEM analysis. As reported, the lattice spacing mismatch as well as the strong metal-support interaction between the metal nanocrystals and supports can induce tensile strain in the metal nanocrystals [36,37]. The generation of tensile strain is probably due to the mismatched lattice spacing and the strong interactions between the Pd nanoparticles and the SnO$_2$ nanotubes. No lattice tensile strains are found in the Pd nanoparticles of the Pd/C sample, which may be attributed to the weak interactions between the carbon supports and the Pd nanocrystals. As reported, the tensile strain generated in the Pd catalyst is beneficial to enhance the ORR activity of the Pd catalyst by lowering the adsorption energies of the reaction intermediates [15,21].

We further carried out XPS measurements to investigate the composition and chemical state of the above two samples. There are distinct characteristic peaks of Pd and SnO$_2$ in the XPS spectrum of the Pd/SnO$_2$ sample, while no characteristic peaks of SnO$_2$ are observed in the spectrum of the Pd/C sample (Fig. 5b and S4). As shown in Fig. 5c, compared with the Pd/C sample, the Pd 3d$_{5/2}$ peak of the Pd/SnO$_2$ sample shows ~ 0.9 eV downshift, suggesting improved electron density of the Pd sites. Meanwhile, the Sn 3d$_{5/2}$ and Sn 3d$_{3/2}$ peaks of the Pd/SnO$_2$ sample exhibit ~ 0.2 eV upshift in comparison with those of the SnO$_2$ sample (Fig. S5). These results reveal the metal-support interactions with electron transfers between the SnO$_2$ support and the Pd nanoparticles. By virtue of the electron-rich feature, the Pd sites can decrease the adsorption energies of the ORR intermediates, thus increasing their ORR activity [38,39].

Electrochemical tests of the Pd/C and Pd/SnO$_2$ catalysts were conducted to reveal the effect of SnO$_2$ and carbon supports on the catalytic performance of the Pd catalyst. In contrast to the cyclic voltammetry (CV) curves recorded in N$_2$-saturated electrolytes

(Fig. 6a and S6), both Pd/C and Pd/SnO$_2$ electrocatalysts have additional reduction peaks in the CV curves tested in O$_2$-saturated electrolytes, suggesting the existence of catalytic oxygen reduction. The ORR activities of these catalysts were further evaluated *via* linear sweep voltammetry (LSV). As shown in Fig. 6b, S7 and S8, the Pd/SnO$_2$ catalyst on glassy carbon electrodes shows a higher half-wave potential of 0.832 V (*vs.* reversible hydrogen electrode, RHE) than that of Pd/C (0.817 V *vs.* RHE). Furthermore, the mass activity of Pd/SnO$_2$ is 0.038 A·mg$_{Pd}^{-1}$, 2.5 times higher than that (0.015 A·mg$_{Pd}^{-1}$) of Pd/C (Fig. 6c). The Tafel slope of Pd/SnO$_2$ is 75.6 mV dec^{-1}, which is greatly lower compared with that (112.4 mV dec^{-1}) of Pd/C (Fig. 6d). The double-layer capacitance tests of catalysts were performed to calculate the electrochemical active surface areas (ECSA) of catalysts [40,41], and then the specific activities of the catalysts were revealed by normalizing the currents to the ECSA values. As shown in Fig. S9 and Table 1, the specific activity (7 × 10^{-3} mA/cm^2) of the Pd/SnO$_2$ catalyst is much higher than that (0.65 × 10^{-3} mA/cm^2) of the Pd/C catalyst. From the Nyquist plots (Fig. S10), the charge transfer resistance (27.5 Ω) of the Pd/SnO$_2$ catalyst is similar to that (28.2 Ω) of the Pd/C catalyst.

We further evaluated the operation durability of the Pd/SnO$_2$ catalyst. During the chronoamperometric test (Fig. 7a), the Pd/SnO$_2$ catalyst exhibited much higher catalytic stability with a low current attenuation rate of 4% after 50 h of continuous operation, compared to that (18%) of commercial Pd/C. The accelerated durability measurement was conducted to further access the catalytic durability of the Pd/SnO$_2$ catalyst (Fig. 7b and S11). Remarkably, its half-wave potential exhibited only 7 mV of negative shift after 30,000 cycles of test. The Pd/SnO$_2$ catalyst in this work exhibited good catalytic stability, which was superior to that of other previously reported Pd-based ORR electrocatalysts (see Table 1)
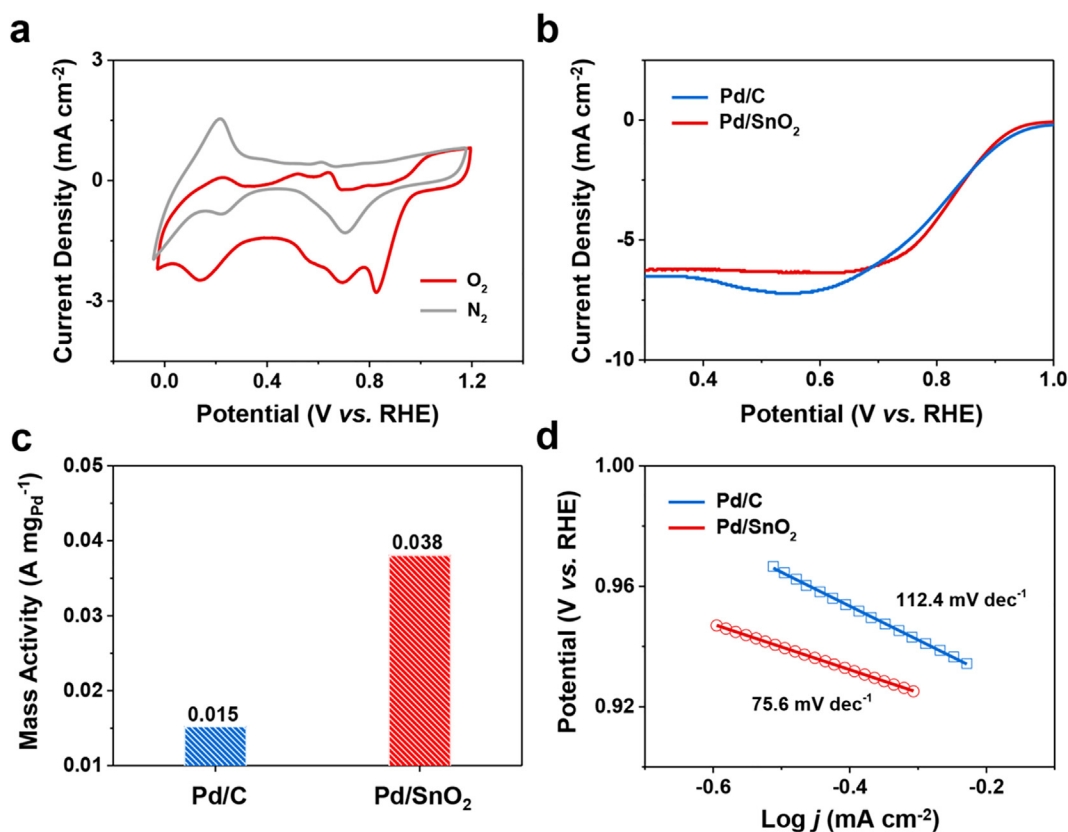

Fig. 6. (a) CV curves of Pd/SnO$_2$ catalyst measured in N$_2$ or O$_2$-saturated aqueous electrolytes. (b) LSV curves, (c) Mass activities and (d) Tafel curves of Pd/SnO$_2$ and Pd/C electrocatalysts measured in O$_2$-saturated aqueous electrolytes.
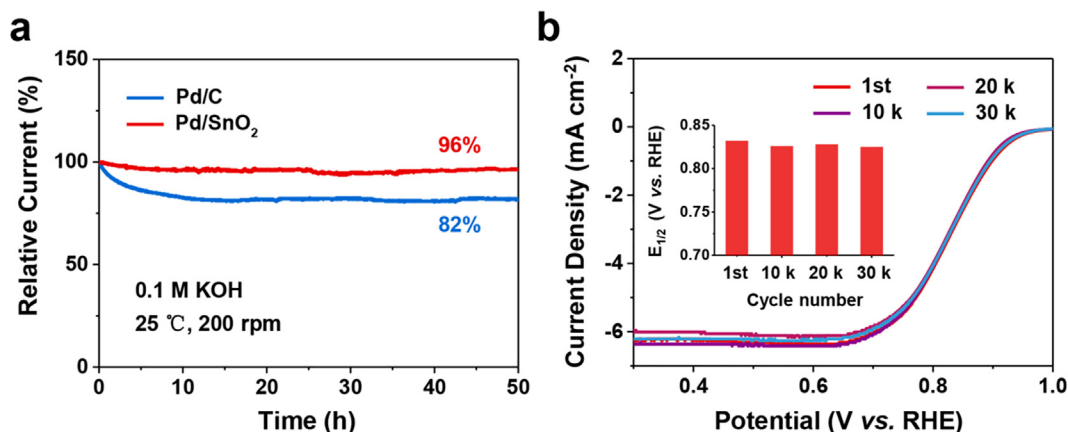
Fig. 7. (a) Chronoamperometric responses of Pd/SnO$_2$ and Pd/C electrocatalysts at 0.7 V (*vs.* RHE). (b) ORR polarization curves of Pd/SnO$_2$ after accelerated durability tests.

Table 1
Comparison of the catalytic stability for Pd/SnO$_2$ and the reported ORR electrocatalysts.

Catalyst	Stability (mass activity loss after different cycles of tests)	Reference
Pd/SnO$_2$	−8.3% (after 30 k, 0.9 V)	This work
Pd/C-10 wt%	−50.8% (after 20 k, 0.9 V)	[42]
PdNCs	−20.5% (after 5 k, 0.9 V)	[43]
Pd-Te HPs/C	−16% (after 20 k, 0.9 V)	[44]
PdCu cube/C	−31.7% (after 30 k, 0.9 V)	[45]
Pt-Ir-Pd	−17.6% (after 5 k, 0.9 V)	[46]
Pd@PdFe	−15% (after 20 k, 0.9 V)	[47]
PdBP MSs	−32.1% (after 5 k, 0.9 V)	[48]
Pd$_4$Sn NWs/C	−9.2% (after 10 k, 0.9 V)	[49]
PtPdCo NRs/C	−29% (after 30 k, 0.9 V)	[50]

[42–50]. The above results prove that the SnO$_2$ support can effectively improve the catalytic activity and stability of a Pd catalyst towards ORR. As reported, Pd-based catalysts could also be used in other catalytic reactions, such as the methanol oxidation reaction (MOR) and the hydrogen evolution reaction (HER) [51–54]. However, these Pd-based catalysts also suffer from some problems including inferior catalytic stability and complicated preparation methods. It is urgently desired to explore efficient methods to synthesize high-performance Pd catalysts. This work demonstrates that a Pd catalyst can obtain tensile-strain and electron-rich features on an SnO$_2$ support, which can promote the catalytic activity and stability of a Pd/SnO$_2$ hybrid catalyst. Thus, an SnO$_2$ support would also be used to prepare high-efficiency Pd-based catalysts for other electrocatalytic reactions (MOR, HER, etc.)

4. Conclusions

In summary, we report an efficient electrocatalyst with Pd nanoparticles anchored onto chemically-stable semiconducting SnO$_2$ nanotubes for the ORR. By combining X-ray diffraction, transmission electron microscopy and X-ray photoelectron spectroscopy, we verified that the SnO$_2$ support can induce tensile strain and electron-rich features in the Pd nanoparticles of a Pd/SnO$_2$ catalyst. In sharp contrast, no such features are found in a Pd/C catalyst with Pd nanoparticles anchored onto the carbon supports. This work reveals that the introduction of SnO$_2$ supports is an effective strategy for the lattice-strain and electron-density modulation of Pd catalysts. Notably, the electrochemical measurements show that the Pd/SnO$_2$ catalyst exhibits a 2.5-fold improvement in mass activity and significantly enhanced catalytic durability towards ORR in comparison with the Pd/C catalyst,

which also outperforms other reported Pd-based catalysts [39–47]. The strategy of constructing Pd/SnO$_2$ hybrid catalysts can overcome the problem of inferior catalytic stability for Pd-based alloy catalysts that would suffer from the unfavorable dealloying and dissolution of metal components during the ORR process [21–23]. This work demonstrates that the SnO$_2$ supports and endowing metal-support interactions are crucial for the enhanced ORR activity and stability of Pd/SnO$_2$ catalyst, which would play an important role in enhancing the catalytic performance of Pd catalysts for other electrocatalytic reactions, including methanol oxidation reaction and hydrogen evolution reaction [51–54]. In a broader context, this work provides insights for further advancement of heterogeneous catalysts with optimal supports in various electrochemical reactions.

CRediT authorship contribution statement

Guojie Chao: Methodology, Writing - original draft. **Longsheng Zhang:** Supervision, Funding acquisition, Writing - review & editing. **Tiantian Xue:** Investigation. **Jing Tian:** Investigation. **Wei Fan:** Funding acquisition, Writing - review & editing. **Tianxi Liu:** Supervision, Funding acquisition, Writing - review & editing.

Declaration of Competing Interest

The authors declare that they have no known competing financial interests or personal relationships that could have appeared to influence the work reported in this paper.

Acknowledgments

Appendix A. Supplementary data

Supplementary data to this article can be found online at https://doi.org/10.1016/j.jcis.2021.05.177.

References

[1] H.T. Chung, J.H. Won, P. Zelenay, Active and stable carbon nanotube/nanoparticle composite electrocatalyst for oxygen reduction, Nat. Commun. 4 (2013) 1922.

[2] X. Tian, X. Zhao, Y.Q. Su, L. Wang, H. Wang, D. Dang, B. Chi, H. Liu, E.J.M. Hensen, X.W.D. Lou, B.Y. Xia, Engineering bunched Pt-Ni alloy nanocages for efficient oxygen reduction in practical fuel cells, Science 366 (2019) 850–856.

[3] D.Y. Chung, J.M. Yoo, Y.E. Sung, Highly durable and active Pt-based nanoscale design for fuel-cell oxygen-reduction electrocatalysts, Adv. Mater. 30 (2018) 1704123.

[4] G. Chao, L. Zhang, D. Wang, S. Chen, H. Guo, K. Xu, W. Fan, T. Liu, Activation of graphitic nitrogen sites for boosting oxygen reduction, Carbon 159 (2020) 611–616.

[5] H. Niu, L. Zhang, J. Feng, Q. Zhang, H. Huang, A. Wang, Graphene-encapsulated cobalt nanoparticles embedded in porous nitrogen-doped graphitic carbon nanosheets as efficient electrocatalysts for oxygen reduction reaction, J. Colloid Interface Sci. 552 (2019) 744–751.

[6] H. Meng, Y. Liu, H. Liu, S. Pei, X. Yuan, H. Li, Y. Zhang, ZIF67@MFC-derived Co/ N-C@CNFs interconnected frameworks with graphitic carbon-encapsulated Co nanoparticles as highly stable and efficient electrocatalysts for oxygen reduction reactions, ACS Appl. Mater. Interfaces 12 (2020) 25961–25971.

[7] X. Wang, M.T. Swihart, G. Wu, Achievements, challenges and perspectives on cathode catalysts in proton exchange membrane fuel cells for transportation, Nat. Catal. 2 (2019) 578–589.

[8] B. Xia, Y. Yan, N. Li, H. Wu, X. Lou, X. Wang, A metal-organic framework-derived bifunctional oxygen electrocatalyst, Nat. Energy 1 (2016) 15006.

[9] T. Zhu, Q. Feng, S. Liu, C. Zhang, Metallogel-derived 3D porous carbon nanosheet composites as an electrocatalyst for oxygen reduction reaction, Compos. Commun. 20 (2020) 100376.

[10] Q. Zhao, X. Tan, T. Ma, F. Cao, Z. Xia, H. Liu, H. Ning, Z. Li, H. Hu, M. Wu, Reinforced atomically dispersed Fe-N-C catalysts derived from petroleum asphalt for oxygen reduction reaction, J. Colloid Interface Sci. 587 (2021) 810–819.

[11] E. Antolini, Palladium in fuel cell catalysis, Energy Environ. Sci. 2 (2009) 915–931.

[12] Q. Xue, G. Xu, R. Mao, H. Liu, J. Zeng, J. Jiang, Y. Chen, Polyethyleneimine modified AuPd@PdAu alloy nanocrystals as advanced electrocatalysts towards the oxygen reduction reaction, J. Energy Chem. 26 (2017) 1153–1159.

[13] M. Shao, T. Yu, J.H. Odell, M. Jin, Y. Xia, Structural dependence of oxygen reduction reaction on palladium nanocrystals, Chem. Commun. 47 (2011) 6566–6568.

[14] H. Li, S. Guo, K. Shin, M.S. Wong, G. Henkelman, Design of a Pd–Au Nitrite Reduction Catalyst by Identifying and Optimizing Active Ensembles, ACS Catal. 9 (2019) 7957–7966.

[15] L. Wang, Z. Zeng, W. Gao, T. Maxson, D. Raciti, M. Giroux, X. Pan, C. Wang, J. Greeley, Tunable intrinsic strain in two-dimensional transition metal electrocatalysts, Science 363 (2019) 870–874.

[16] J.k. Nørskov, J. Rossmeisl, A. Logadottir, L. Lindqvist, Origin of the overpotential for oxygen reduction at a fuel-cell cathode, J. Phys. Chem. B 108 (2004) 17886–17892.

[17] F.H.B. Lima, J. Zhang, M.H. Shao, K. Sasaki, M.B. Vukmirovic, E.A. Ticianelli, R.R. Adzic, Catalytic activity-d-band center correlation for the O_2 reduction reaction on platinum in alkaline solutions, J. Phys. Chem. C 111 (2007) 404–410.

[18] Y. Suo, L. Zhuang, J. Lu, First-principles considerations in the design of Pd-alloy catalysts for oxygen reduction, Angew. Chem., Int. Ed. 46 (2007) 2920–2922.

[19] M. Luo, Z. Zhao, Y. Zhang, Y. Sun, Y. Xing, F. Lv, Y. Yang, X. Zhang, S. Hwang, Y. Qin, J.-Y. Ma, F. Lin, D. Su, G. Lu, S. Guo, PdMo bimetallene for oxygen reduction catalysis, Nature 574 (2019) 81–85.

[20] Y. Feng, Q. Shao, Y. Ji, X. Cui, Y. Li, X. Zhu, X. Huang, Surface-modulated palladium-nickel icosahedra as high-performance non-platinum oxygen reduction electrocatalysts, Sci. Adv. 4 (2018) eaap8817.

[21] J. Lin, C. Xi, Z. Li, Y. Feng, D. Wu, C. Dong, P. Yao, H. Liu, X. Du, Lattice-strained palladium nanoparticles as active catalysts for the oxygen reduction reaction, Chem. Commun. 55 (2019) 3121–3123.

[22] M. Escudero-Escribano, P. Malacrida, M.H. Hansen, U.G. Vej-Hansen, A. Velazquez-Palenzuela, V. Tripkovic, J. Schiotz, J. Rossmeisl, I.E.L. Stephens, I. Chorkendorff, Tuning the activity of Pt alloy electrocatalysts by means of the lanthanide contraction, Science 352 (2016) 73–76.

[23] M. Asano, R. Kawamura, R. Sasakawa, N. Todoroki, T. Wadayama, Oxygen reduction reaction activity for strain-controlled Pt-based model alloy catalysts: surface strains and direct electronic effects induced by alloying elements, ACS Catal. 6 (2016) 5285–5289.

[24] J. Ftouni, A. Munoz-Murillo, A. Goryachev, J.P. Hofmann, E.J.M. Hensen, L. Lu, C. J. Kiely, P.C.A. Bruijnincx, B.M. Weckhuysen, ZrO_2 is preferred over TiO_2 as support for the Ru-catalyzed hydrogenation of levulinic acid to gamma-valerolactone, ACS Catal. 6 (2016) 5462–5472.

[25] S.J. Tauster, S.C. Fung, R.T. Baker, J.A. Horsley, Strong interactions in supported-metal catalysts, Science 211 (1981) 1121–1125.

[26] D. Nechiyil, M.S. Garapati, R.C. Shende, S. Joulie, D. Neumeyer, R. Bacsa, P. Puech, S. Ramaprabhu, W. Bacsa, Optimizing metal-support interphase for efficient fuel cell oxygen reduction reaction catalyst, J. Colloid Interface Sci. 561 (2020) 439–448.

[27] L. Li, L. Hu, J. Li, Z. Wei, Enhanced stability of Pt nanoparticle electrocatalysts for fuel cells, Nano Res. 8 (2015) 418–440.

[28] L. Zhang, L. Wang, H. Lin, Y. Liu, J. Ye, Y. Wen, A. Chen, L. Wang, F. Ni, Z. Zhou, S. Sun, Y. Li, B. Zhang, H. Peng, A lattice-oxygen-involved reaction pathway to boost urea oxidation, Angew. Chem., Int. Ed. 58 (2019) 16820–16825.

[29] F.B. Ometto, E.A. Carbonio, E. Teixeira-Neto, H.M. Villullas, Changes induced by transition metal oxides in Pt nanoparticles unveil the effects of electronic properties on oxygen reduction activity, J. Mater. Chem. A 7 (2019) 2075–2086.

[30] J. Li, S. You, M. Liu, P. Zhang, Y. Dai, Y. Yu, N. Ren, J, Zou, ZIF-8-derived carbon-thin-layer protected $WC/W_{24}O_{68}$ micro-sized rods with enriched oxygen vacancies as efficient Pt co-catalysts for methanol oxidation and oxygen reduction, Appl. Catal. B: Environ. 265 (2020) 118574.

[31] G. Cognard, G. Ozouf, C. Beauger, G. Berthome, D. Riassetto, L. Dubau, R. Chattot, M. Chatenet, F. Maillard, Benefits and limitations of Pt nanoparticles supported on highly porous antimony-doped tin dioxide aerogel as alternative cathode material for proton-exchange membrane fuel cells, Appl. Catal. B: Environ. 201 (2017) 381–390.

[32] M. Nakada, A. Ishihara, S. Mitsushima, N. Kamiya, K.-I. Ota, Effect of tin oxides on oxide formation and reduction of platinum particles, Electrochem. Solid-State Lett. 10 (2007) F1–F4.

[33] P. Zhang, S.Y. Huang, B.N. Popov, Mesoporous tin oxide as an oxidation-resistant catalyst support for proton exchange membrane fuel cells, J. Electrochem. Soc. 157 (2010) B1163–B1172.

[34] X. Shen, T. Nagai, F. Yang, L. Zhou, Y. Pan, L. Yao, D. Wu, Y. Liu, J. Feng, J. Guo, H. Jia, Z. Peng, Dual-site cascade oxygen reduction mechanism on $SnO_x/Pt-Cu-Ni$ for promoting reaction kinetics, J. Am. Chem. Soc. 141 (2019) 9463–9467.

[35] Y. Huang, Y. Miao, L. Zhang, W.W. Tjiu, J. Pan, T. Liu, Synthesis of few-layered MoS_2 nanosheet-coated electrospun SnO_2 nanotube heterostructures for enhanced hydrogen evolution reaction, Nanoscale 6 (2014) 10673–10679.

[36] W. Zhu, H. Yuan, F. Liao, Y. Shen, H. Shi, Y. Shi, L. Xu, M. Ma, M. Shao, Strain engineering for Janus palladium-gold bimetallic nanoparticles: enhanced electrocatalytic performance for oxygen reduction reaction and zinc-air battery, Chem. Eng. J. 389 (2020) 124240.

[37] J.H. Kim, S. Chang, Y.T. Kim, Compressive strain as the main origin of enhanced oxygen reduction reaction activity for Pt electrocatalysts on chromium-doped titania support, Appl. Catal., B 158 (2014) 112–118.

[38] J. Li, H. Zhou, H. Zhuo, Z. Wei, G. Zhuang, X. Zhong, S. Deng, X. Li, J. Wang, Oxygen vacancies on TiO_2 promoted the activity and stability of supported Pd nanoparticles for the oxygen reduction reaction, J. Mater. Chem. A 6 (2018) 2264–2272.

[39] S. Hussain, N. Kongi, H. Erikson, M. Rähn, M. Merisalu, L. Matisen, P. Paiste, J. Aruvali, V. Sammelselg, L.A. Estudillo-Wong, K. Tammeveski, N. Alonso-Vante, Platinum nanoparticles photo-deposited on SnO_2-C composites: an active and durable electrocatalyst for the oxygen reduction reaction, Electrochim. Acta 316 (2019) 162–172.

[40] N. Song, S. Hong, M. Xiao, Y. Zuo, E. Jiang, C. Li, H. Dong, Fabrication of Co(Ni)-P surface bonding states on core-shell $Co(OH)_2$@P-NiCo-LDH towards electrocatalytic hydrogen evolution reaction, J. Colloid Interface Sci. 582 (2021) 535–542.

[41] Y.T. Kim, P.P. Lopes, S.A. Park, A.Y. Lee, J. Lim, H. Lee, S. Back, Y. Jung, N. Danilovic, V. Stamenkovic, J. Erlebacher, J. Snyder, N.M. Markovic, Balancing activity, stability and conductivity of nanoporous core-shell iridium/iridium oxide oxygen evolution catalysts, Nat. Commun. 8 (2017) 1449.

[42] C. Tang, N. Zhang, Y. Ji, Q. Shao, Y. Li, X. Xiao, X. Huang, Fully tensile strained Pd_3Pb/Pd tetragonal nanosheets enhance oxygen reduction catalysis, Nano Lett. 19 (2019) 1336–1342.

[43] L. Sahoo, U.K. Gautam, Boosting bifunctional oxygen reduction and methanol oxidation electrocatalytic activity with 2D superlattice-forming Pd nanocubes generated by precise acid etching, ACS Appl. Nano Mater. 3 (2020) 8117–8125.

[44] Y. Zhang, B. Huang, G. Luo, T. Sun, Y. Feng, Y. Wang, Y. Ma, Q. Shao, Y. Li, Z. Zhou, X. Huang, Atomically deviated Pd-Te nanoplates boost methanol-tolerant fuel cells, Sci. Adv. 6 (2020) eaba9731.

[45] Q. Zhang, F. Li, L. Li, J. Peng, W. Zhang, W. Chen, Q. Xiang, F. Shi, W. Shang, P. Tao, C. Song, R. Huang, H. Zhu, T. Deng, J. Wu, Boosting oxygen and peroxide reduction reactions on PdCu intermetallic cubes, ChemElectroChem 7 (2020) 2614–2620.

[46] J. Zhu, M. Xie, Z. Chen, Z.H. Lyu, M.F. Chi, W. Jin, Y. Xia, Pt-Ir-Pd trimetallic nanocages as a dual catalyst for efficient oxygen reduction and evolution reactions in acidic media, Adv. Energy Mater. 10 (2020) 1904114.

[47] X. Li, X. Li, C. Liu, H. Huang, P. Gao, F. Ahmad, L. Luo, Y. Ye, Z. Geng, G. Wang, R. Si, C. Ma, J. Yang, J. Zeng, Atomic-level construction of tensile-strained PdFe alloy surface toward highly efficient oxygen reduction electrocatalysis, Nano Lett. 20 (2020) 1403–1409.

[48] H. Lv, D. Xu, L. Sun, J. Henzie, S.L. Suib, Y. Yamauchi, B. Liu, Ternary palladium-boron-phosphorus alloy mesoporous nanospheres for highly efficient electrocatalysis, ACS Nano 13 (2019) 12052–12061.

[49] Y. Zhang, B. Huang, Q. Shao, Y. Feng, L. Xiong, Y. Peng, X. Huang, Defect engineering of palladium-tin nanowires enables efficient electrocatalysts for fuel cell reactions, Nano Lett. 19 (2019) 6894–6903.

[50] Y. Sun, X. Zhang, M. Luo, X. Chen, L. Wang, Y. Li, M. Li, Y. Qin, C. Li, N. Xu, G. Lu, P. Gao, S. Guo, Ultrathin PtPd-based nanorings with abundant step atoms enhance oxygen catalysis, Adv. Mater. 30 (2018) 1802136.

[51] L.S.R. Silva, C.V.S. Almeida, C.T. Meneses, E.A. Batista, S.F. Santos, K.I.B. Eguiluz, G.R. Salazar-Banda, AuPd/C core-shell and alloy nanoparticles with enhanced catalytic activity toward the electro-oxidation of ethanol in alkaline media, Appl. Catal. B 251 (2019) 313–325.

[52] X. Zhang, P. Yang, S. Jiang, Pd nanoparticles assembled on Ni- and N-doped carbon nanotubes towards superior electrochemical activity, Int. J. Hydrogen Energy 46 (2021) 2065–2074.

[53] H. Chen, M. Jin, L. Zhang, A. Wang, J. Yuan, Q. Zhang, J. Feng, One-pot aqueous synthesis of two-dimensional porous bimetallic PtPd alloyed nanosheets as highly active and durable electrocatalyst for boosting oxygen reduction and hydrogen evolution, J. Colloid Interface Sci. 543 (2019) 1–8.

[54] Y. Liu, W. Li, G. Zhao, G. Qin, Y. Li, Y. Liu, Self-driven microstructural evolution of Au@Pd core-shell nanoparticles for greatly enhanced catalytic performance during methanol electrooxidation, Nanoscale 13 (2021) 3528–3542.